Magnetic Fe_3O_4-natural iron ore/calcium alginate beads as heterogeneous catalyst for Novacron blue dye degradation in water by (photo)Fenton process

Sirine Ben Ayed[1], Lamjed Mansour[2], Vincenzo Vaiano[3], Abdel Halim Harrath[2], Fadhila Ayari[1]*, Luigi Rizzo[4*]

[1]Faculty of Sciences of Bizerte, LR 05/ES09 Laboratory of Applications of Chemistry to Resources and Natural Substances and to the Environment (LACReSNE), Carthage University, Zarzouna 7021, Tunisia, email: sirinebenayed19@gmail.com

[2]Zoology Department, College of Science, King Saud University, Riyadh, Saudi Arabia, email: lmansour@ksu.edu.sa

[3]Department of Industrial Engineering, University of Salerno, Via Giovanni Paolo II 132, 84084 Fisciano (SA), Italy, email: vvaiano@unisa.it

[4]Water Science and Technology group (WaSTe), Department of Civil Engineering, University of Salerno, Via Giovanni Paolo II 132, 84084, Fisciano (SA), Italy

Post-review version of the manuscript published in Journal of Photochemistry & Photobiology, 16 A: Chemistry 438 (2023) 114566, https://doi.org/10.1016/j.jphotochem.2023.114566

* Corresponding authors: fadhilaayari@yahoo.fr (F.A.); l.rizzo@unisa.it (L.R.)

Abstract

Purposely prepared magnetic nanocomposite beads were investigated as catalysts for the degradation of Novacron blue (NB) dye (a reactive azo dye widely used in textile industries) by Fenton and photo-Fenton processes. Specifically, magnetic Fe_3O_4 nanoparticles and natural iron ore (NIO) were incorporated into sodium calcium alginate material to form Fe_3O_4-NIO calcium alginate beads using an inexpensive protocol. While Fe_3O_4/calcium alginate beads might be a good catalyst for Fenton and photo-Fenton processes, adding NIO could be beneficial to enhance the stability of the magnetic beads. The as-prepared catalyst was characterized by several techniques such as Fourier transform infrared spectroscopy (FT-IR), X-ray diffraction (XRD), Brunauer, Emmett and Teller (BET) and Barret-Joyner-Halender (BJH), scanning electron microscopy (SEM), transmission electron microscopy (TEM), energy dispersive X-ray spectroscopy (EDX) and UV-Vis diffuse reflectance analyses. Such characterizations showed that the (photo)catalyst was successfully synthesized, as well as its porous nature with a specific surface area of 26 m^2/g. Magnetic nanocomposite alginate beads showed adsorptive properties by removing 22% of NB dye under optimum conditions (pH 2, $[NB]_0$=40mg/L, and 0.2g dose of beads). This magnetic catalyst proved a great photocatalytic behavior according to its optical properties and contributed as a photo-Fenton catalyst to the degradation of 80% of NB dye after 120 min treatment compared to only 50% after 120 min of Fenton process. This cheap, eco-friendly, non-toxic, magnetically separable and stable catalyst was reused for six subsequent photo-Fenton tests. All these advantages show its potential to be used as heterogeneous catalyst in wastewater treatment applications making it worthy of further investigation under more realistic conditions.

Keywords: Fenton; magnetic nanocomposite; photo-Fenton; textile wastewater; wastewater treatment

1. **Introduction**

Textile dyes are highly toxic compounds that have always been a source of serious harm to the ecosystem for many decades. Among these dyes, Novacron blue (NB) dye is ranked as one of the most harmful dyes due to its mutagenic and carcinogenic effects on living organisms [1]. This reactive azo dye, characterized by the chromophore group –N=N– presence, is known for its stability only in acidic medium [2, 3]. NB dye is extensively used in most of the textile industries in Tunisia owing to its high stability and its simple dying protocol despite being refractory to conventional wastewater treatment processes, such as biological [4,5], chemical [6] and physical [7] ones. Therefore, it is very crucial to apply a suitable and effective process to treat textile wastewater before disposal into the aquatic environment.

Advanced oxidation processes (AOPs) are very efficient and promising technologies that are based on the generation of highly reactive species, such as ·OH**,** to oxidize target pollutants [8, 9,10,11]. These processes have proven to be very effective to degrade various pollutants in wastewater [12,13,14]. Among all, Fenton and photo-Fenton processes have been always a subject of interest regarding their ability to degrade different pollutants occurring in water and wastewater. The core of Fenton and photo Fenton processes is the reaction between iron, as a catalyst, H_2O_2, as oxidant, and a source of irradiation (photo-Fenton case) to produce highly reactive species such as hydroxyl radical (·OH) [15,16].

Heterogeneous Fenton and photo-Fenton processes are an attractive option for water and wastewater treatment because of different advantages compared to the homogeneous respective processes, such as the easy recovery and the reusability of the catalyst and the absence of sludge formation [17,18].

Alginate is a biopolymer commonly extracted from marine brown algae and consisting of α-(1 → 4)-linked l-guluronic acid (G) and β-(1 → 4)-linked d-mannuronic acid (M) units with different G:M ratio [19,10]. Its (G)unit has a better affinity to calcium ions than (M) unit which is the core of the egg-box phenomenon [21,22]. For a better understanding, Ca^{2+}cations can replace Na^{+} ions existing in the guluronic acid unit to give a crosslinked hydrogel model called "egg-boxes" [23,24]. This natural polymer has been used widely as a support to encapsulate drugs [25], proteins [26]and enzymes [27]. Moreover, the carboxylate functions in the alginate matrix guarantee an effective binding to other elements leading to the development of different alginate based materials. Due to its non-toxicity, abundance, low cost and good adsorptive performance against contaminants, alginate has attracted the attention of many researchers as a

support matrix of catalysts in water treatment applications [28,29,30]. However, research papers that deal with incorporated adsorbent-photocatalyst material are still quite limited.

On the other hand, iron oxides are very effective candidates to be used in AOPs applications to water and wastewater treatment due to their high chemical stability, non-toxicity and their photocatalytic activity [31,32].

In this study, Fe_3O_4 nanoparticles and natural iron oxide were successfully embedded in alginate matrix to form Fe_3O_4-NIO/calcium alginate beads to be used as heterogeneous catalysts in Fenton and photo-Fenton processes for the degradation of NB reactive azo dye. The reason of using natural iron ore in the synthesis of magnetic nanocomposite alginate beads was to enhance the stability of the beads and to make them stiffer and stronger to prevent their breakage during treatment. Additionally, the presence of Fe in the catalyst is improved through a natural source which leads to an increase in the photocatalytic activity of the beads against the target pollutants. To the author's best knowledge, no study has reported the same developed systems (Fe_3O_4-NIO/calcium alginate beads/H_2O_2 and Fe_3O_4-NIO/calcium alginate beads/H_2O_2/ UVC) to degrade the reactive azo dye NB.

2. Materials and methods

2.1Chemicals and catalyst preparation

2.1.1Chemicals

Sodium alginate was purchased from Sigma–Aldrich (USA). Calcium chloride hexahydrate ($CaCl_2 \cdot 6H_2O$), ferrous sulphate heptahydrate ($FeSO_4 \cdot 7H_2O$)98%, Ferric chloride ($FeCl_3 \cdot 6H_2O$) 97%, ammonium hydroxide (28%), Hydrogen peroxide (H_2O_2) 30%,Titanium (IV) oxysulfate, Sulfuric acid (H_2SO_4) 96%, Sodium hydroxide (NaOH) 99%, were provided by Carlo Erba. All solutions were prepared in Milli-Q water. The pH was regulated by adding 0.1 M HCl or 0.1M NaOH solutions. The natural iron oxide (NIO) used in this work was characterized in our previous study [33] and it consists of these main elements: magnetite, hematite, goethite, kaolinite and quartz. NB dye was provided by a Tunisian textile industry (SITEX). Stock solution was prepared by dissolving 1g of NB dye in 1000 mL of Milli-Q water, and then stored in opaque bottle for further use to prepare dye solutions with different concentrations. All chemicals used in this study were directly utilized without any further purification.

2.1.2. Preparation of Fe_3O_4 nanoparticles

The synthesis of Fe_3O_4 nanoparticles was carried out by reverse co-precipitation method; according to the procedure reported in our previous work [33]. The obtained nanoparticles were then dispersed in 100mLofMilli-Q water.

2.1.3. Preparation of the magnetic Fe_3O_4-NIO/calcium alginate beads

The Fe_3O_4-NIO/calcium alginate beads were synthesized based on the ionic gelation method (Figure 1) [34,35]. In detail, 1g of NIO was added to the previous magnetite solution and mixed using a magnetic stirrer for 60 min for complete homogenization. Beads were prepared by adding 1g of sodium alginate to the Fe_3O_4-NIO mixture, keeping it under vigorous agitation for four hours to ensure the homogeneity of the solution until no air bubbles appeared. Thereafter, the resultant mixture was poured drip-wise into a magnetically-stirred solution of calcium chloride (0.1M) using a syringe. As soon as it contacts the cross-linking solution ($CaCl_2$), the Fe_3O_4-NIO/alginate gel was transformed into uniform and spherical nanocomposite alginate beads. The obtained beads were left in the solution for 24 h (curing time) to allow the polymerization reaction to complete. It is worth mentioning that, after curing time, the $CaCl_2$ solution is colorless indicating the formation of a protective membrane during the interaction between alginate and Ca^{2+} ions that improves the stability of the beads and do not allow the leaching of the incorporated materials (Fe_3O_4 and NIO) from the beads [36]. All beads were washed several times with distilled water to remove the non-reacted calcium ions, dried at 60 °C overnight and stored in the dark. For characterization purposes, bare calcium alginate beads were prepared also by the same method described above without adding the Fe_3O_4-NIO mixture. In detail, 1g of sodium alginate was added to 100 mL of Milli-Q water and mixed using a stirrer for 60 minutes. Then, the resultant gel was poured in calcium chloride solution (0.1M) using a syringe. Thereafter, the formed beads were left in the $CaCl_2$ solution for 24 hours. Finally, all beads were washed several times with distilled water and dried at 60 °C overnight.

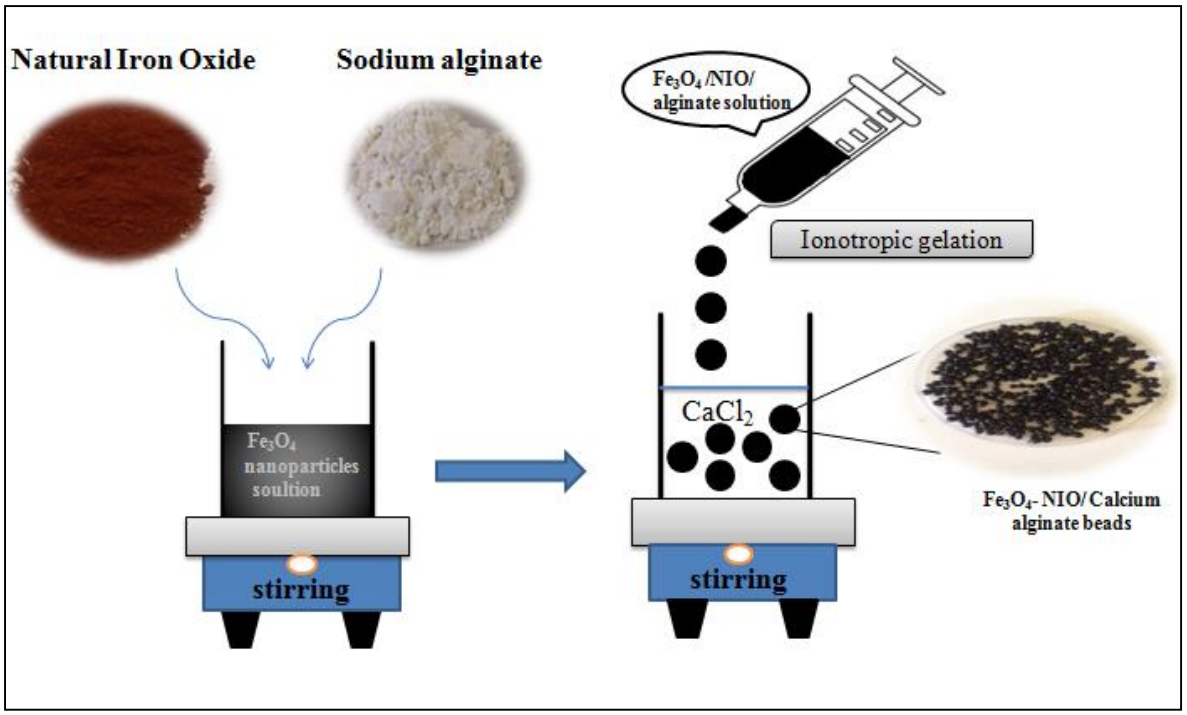

142

143 **Figure 1**: preparation of Fe_3O_4-NIO/calcium alginate beads.

144 **2.1.4. Magnetic properties**

145 The prepared nanocomposite alginate beads can be easily and quickly collected through a
146 magnet within 5 sec (Figure 2). This magnetic behavior facilitates the removal of the catalyst
147 from the aqueous solution.

148

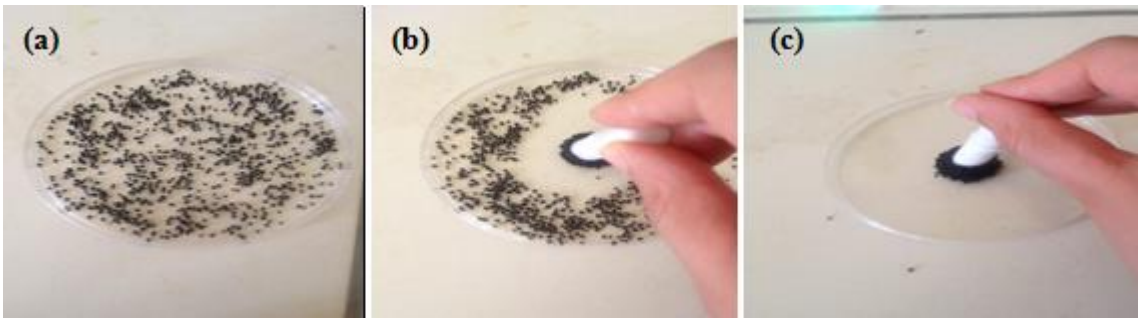

149
150 **Figure 2**: magnetic Fe_3O_4-NIO/calcium alginate beads: (a) without magnetic field, (b) after 2s
151 and (c) after 5s of attraction by a magnetic field

152

153 **2.2. Chemical-physical characterization of the catalysts**

154 Prepared beads were characterized by several techniques. Namely, FT-IR analysis in the range
155 400–4000 cm^{-1}, using a Perkin Elmer 100 FT-IR spectrometer and X-ray diffraction technique

(XRD), using a PANalyticalX'Pert HighScore Plus diffractometer, with monochromatic Cu-K radiation source (λ = 1.5418 Å) operated at 40 kV and 40 mA, were used to characterize the chemical structure of the pure calcium alginate beads and Fe_3O_4-NIO/calcium alginate beads. The morphological structure of the beads was identified by scanning electron microscope (Assing, mod. LEO 420) operated at 3 kV and transmission electron microscopy (JEOL JEM 2100). Energy dispersive X-ray microanalysis (EDX) was used to perform the quantitative analysis of the elemental composition of the beads. Their porosity properties were characterized by N_2 adsorption-desorption at -196 °C using a Quantachrome model Nova 1000e surface and porosity analyzer after pretreatment of the sample at 100 °C for 6h in He flow. Specific surface area of each sample was calculated by Brunauer-Emmett-Teller (BET) method while the total volume pore and the average pore diameter were calculated by Barrett-Joyner-Halenda (BJH) method. Optical properties were examined by UV-vis diffuse reflectance analysis and the spectra of the beads were recorded by a Perkin Elmer spectrometer Lambda 35 using a RSAPE-20 reflectance spectroscopy accessory (Lab sphere Inc., North Sutton, NH).

2.3. Adsorption study and AOPs experimental set up

Dark adsorption tests were initially performed by putting 100 mL of NB dye aqueous solution in contact with a certain dose of beads in the dark under magnetic agitation for 120 min. The concentration of the dye was controlled throughout the adsorption reaction until achieving a saturation stable value. As the required contact time was evaluated, the influence of different parameters such as pH (2-8), catalyst mass (0.1-0.4 g) and dye initial concentration (10-40 mg/L) on the adsorption process was investigated. Each experiment was performed by varying the specific parameter while keeping the others parameters constants. Therewithal, the adsorption tests were carried under the optimum conditions to remove the maximum amount of dye before starting the AOP.

All AOPs tests were performed inside a wooden box (width= 50 cm, length= 50 cm and height= 50 cm) to prevent the penetration of any other source of light. A photo reactor system, composed of borosilicate crystallizing dish filled with NB dye solution under magnetic stirring and UVC lamp as light source (16 W, peak wavelength at 254 nm, intensity of 4.9 mW/cm^2, Sankyo Denky G10T5L, Japan), fixed at 10 cm height above the solution, were placed inside the box.

NB dye degradation was evaluated under different treatment conditions (namely, photolysis, H_2O_2, catalyst/H_2O_2, and UVC/catalyst/H_2O_2) to recognize the real contribution of the prepared nanocomposite beads in the degradation process. For photolysis test, 100 mL of NB dye (40mg/L) aqueous solution at pH 2 was irradiated by only UVC light for 90 min and the samples were taken every 20 min for analysis. The direct oxidation of NB dye in the dark was performed to evaluate the direct influence of H_2O_2 on the NB dye degradation. Fenton and photo-Fenton processes started immediately after 60 min of dark adsorption reaction. In a typical Fenton reaction, H_2O_2 was added to the solution and the samples were collected every 20 min for 120min. Photo-Fenton tests were carried out using UVC light in addition to the conditions and experimental set-up explained for the Fenton process.

All performed experiments were repeated twice to ensure the accuracy of the process.

2.4. Reusability study

The possibility of reusing the catalyst is crucial for possible full scale application of the investigated process. Therefore, six subsequent experiments were carried out using the same magnetic beads that were magnetically collected after every photo-Fenton test, while keeping the same operating conditions. It is worthy to note that the beads were washed with distilled water and dried using absorbent paper sheets after each treatment cycle.

2.5. Analytical measurements

NB dye behavior was monitored throughout the experiments by measuring the absorbance at the dye's maximum absorption wavelength (λ= 609 nm) using a UV-vis spectrophotometer (Perkin Elmer Model T60U PG Instruments Ltd). Hydrogen peroxide concentration was monitored during the reaction according to DIN 38 409H15 method, using Titanium oxysulfate to form pertitanic acid. A pH meter edge® (HANNA, model: HI2020-02) was used to measure the pH of the aqueous solutions.

3. Results and Discussion

3.1. Characterization of the catalysts

3.1.1 FT-IR analysis

The FT-IR spectrum of the nanocomposite alginate beads (Figure 3) reveals a broad and intense band at around 3370 cm^{-1} compared to the low band of the bare calcium alginate beads. This intense and broad band can be ascribed to the overlap of O–H stretching vibration of hydroxyl groups in the alginate chain and O–H stretching vibration in the nanoparticles and NIO [37,38,39]. Both bands at 2930 cm^{-1} and 2846 cm^{-1} are ascribed to aliphatic -CH stretching vibrations [19]. Bands observed at 1640 cm^{-1} and 1400 cm^{-1}can be assigned to the asymmetric and symmetric C=O vibrations of the carboxylic functional groups $-COO^-$ in alginate, respectively [40,41] or to the O-H stretching vibration in Fe_3O_4 nanoparticles [42]. The band at around 1110 $cm^{-1}$is attributed to C–O and COC stretching vibrations [19,43, 44]. The band at around 500 cm^{-1} is associated to the stretching vibration of O-Fe-O functional groups existing in the Fe_3O_4 nanoparticles and the natural iron oxide [43,45], which plays an essential role in the photocatalytic activity [46,47]. These results prove the successful encapsulation of both parent materials in the alginate biopolymer matrix.

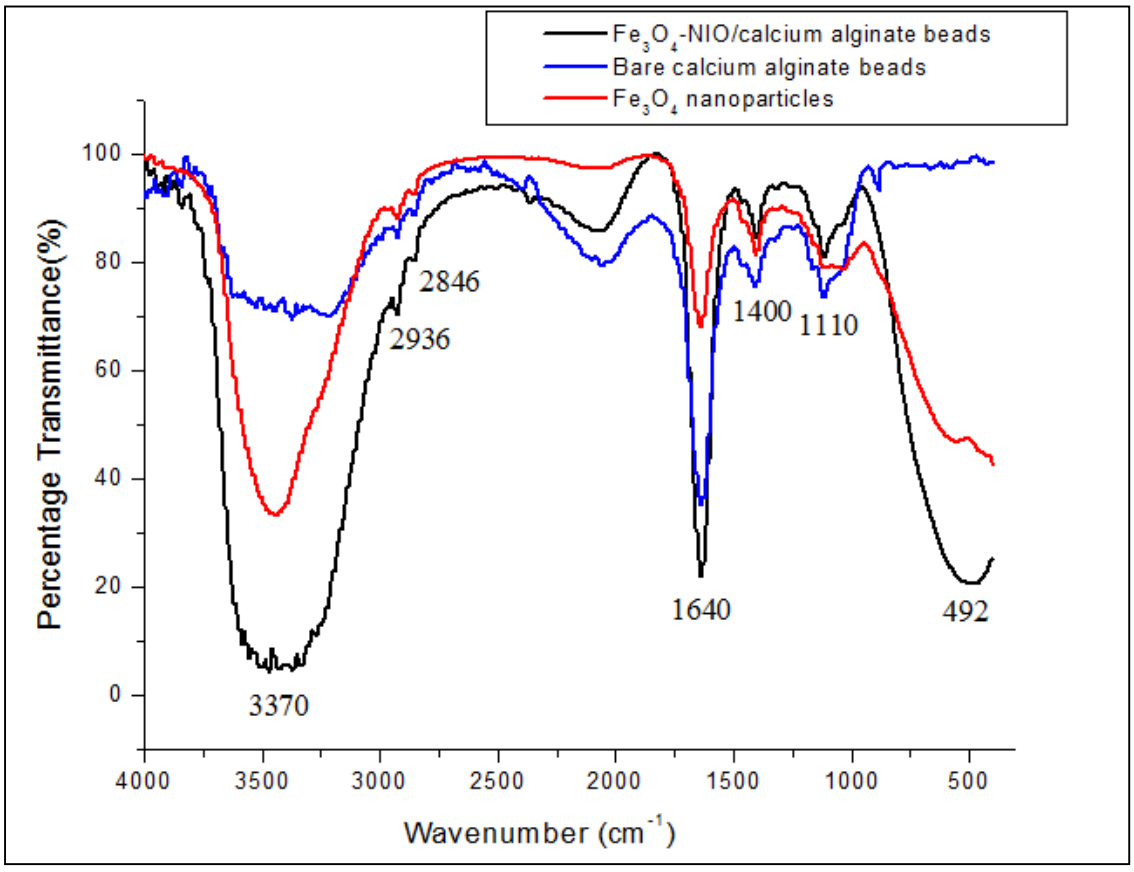

Figure 3: FT-IR spectra of bare calcium alginate beads, Fe_3O_4-NIO/calcium alginate beads and Fe_3O_4 nanoparticles.

3.1.2 XRD analysis

XRD pattern of the calcium alginate beads shows only three weak diffraction peaks at 2Θ =13.43, 22.53 and 37° without any other prominent sharp diffraction peak (Figure 4), which indicates the semi-crystallinity of the studied biopolymer [19] and making these findings consistent with previous studies [38,48,49]. XRD pattern of pure Fe_3O_4 (Figure 4) shows six diffraction peaks at 2Θ = 63.38, 57.77, 54.31, 43.62, 36.09 and 30.65° which coincide with their respective planes (440) (511) (422), (400), (311) and (220) of its spinel structure (JCPDS file No. 19-0629) [50]. The XRD pattern of the nanocomposite alginate beads (Figure 4) shows the major six characteristic peaks of Fe_3O_4, with a slight shift owing to the strong interaction between the nanoparticles and carboxylate groups of alginate, and other peaks at 2Θ= 14.89, 17.77, 21.21, 24.24, 26.61, 28.89, 45.76 and 50.27°, related to FeOOH, Fe_2O_3 and quartz existing in the natural iron oxide which were reported separately in our previous study [33]. Thus, the XRD pattern of Fe_3O_4-NIO/calcium alginate beads basically contains all the characteristic peaks of Fe_3O_4 and NIO materials. These results are in agreement with FT-IR analysis and underline that the biopolymer has no impact on the crystalline nature of the embedded materials [51].

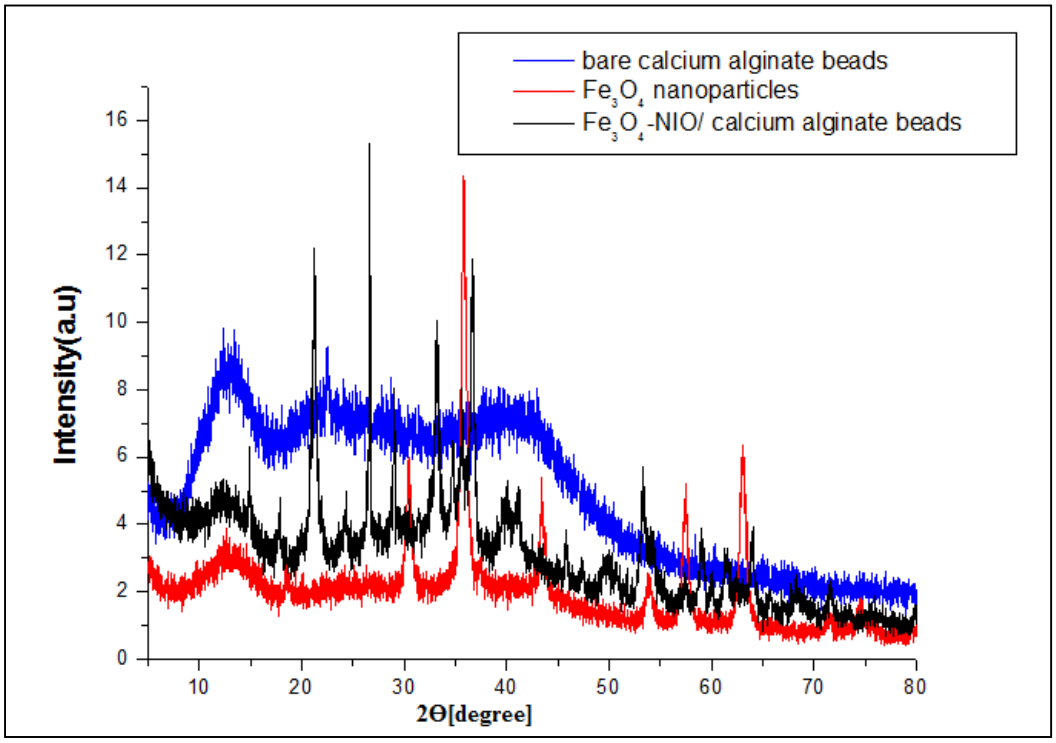

Figure 4: XRD patterns of Fe_3O_4 nanoparticles, bare calcium alginate beads and the hybrid beads.

3.1.3 SEM, TEM and EDX analyses

It is well-known that the morphology and internal structure properties of any catalyst crucially affect its catalytic performance. Thereby, morphological characterization of bare calcium alginate beads and Fe_3O_4-NIO/calcium alginate beads were investigated through the support of SEM. SEM images reveal a surface morphology of calcium alginate beads different compared to the prepared nanocomposite beads**.** In particular, beads are characterized by a rough and cracked surface with some wrinkles yet without much porosity even at higher magnifications (Figure 5a, b, c**)**. These characteristics and properties could be a consequence of the drying step [39]. Similar findings were reported in previous studies on calcium alginate beads [39,52,53,54]. Compared to the above observations, SEM images of Fe_3O_4-NIO/calcium alginate beads display a rougher coarse surface morphology with more pores and cracks and heterogeneous nature (Figure 5d, e, f). The dispersion of natural iron oxide and Fe_3O_4 nanoparticles can be clearly appreciated in Figure 5e, which confirms the successful incorporation of both materials in the alginate beads. In addition to that, the change of beads color from yellow (Figure5g) to black (Figure 5f), owing to the presence of the black Fe_3O_4 nanoparticles and the natural iron ore, is indicative of its effective entrapment in calcium alginate. The enhancement of the surface roughness and porosity of this incorporated framework indicates the improvement of the beads surface area which leads to more binding sites and more available catalytically active sites for a better pollutants degradation [55]. Similar findings were reported by Bilici et al [52] in a paper dealing with the synthesis of hybrid ZnO/ Fe_3O_4 calcium alginate beads.

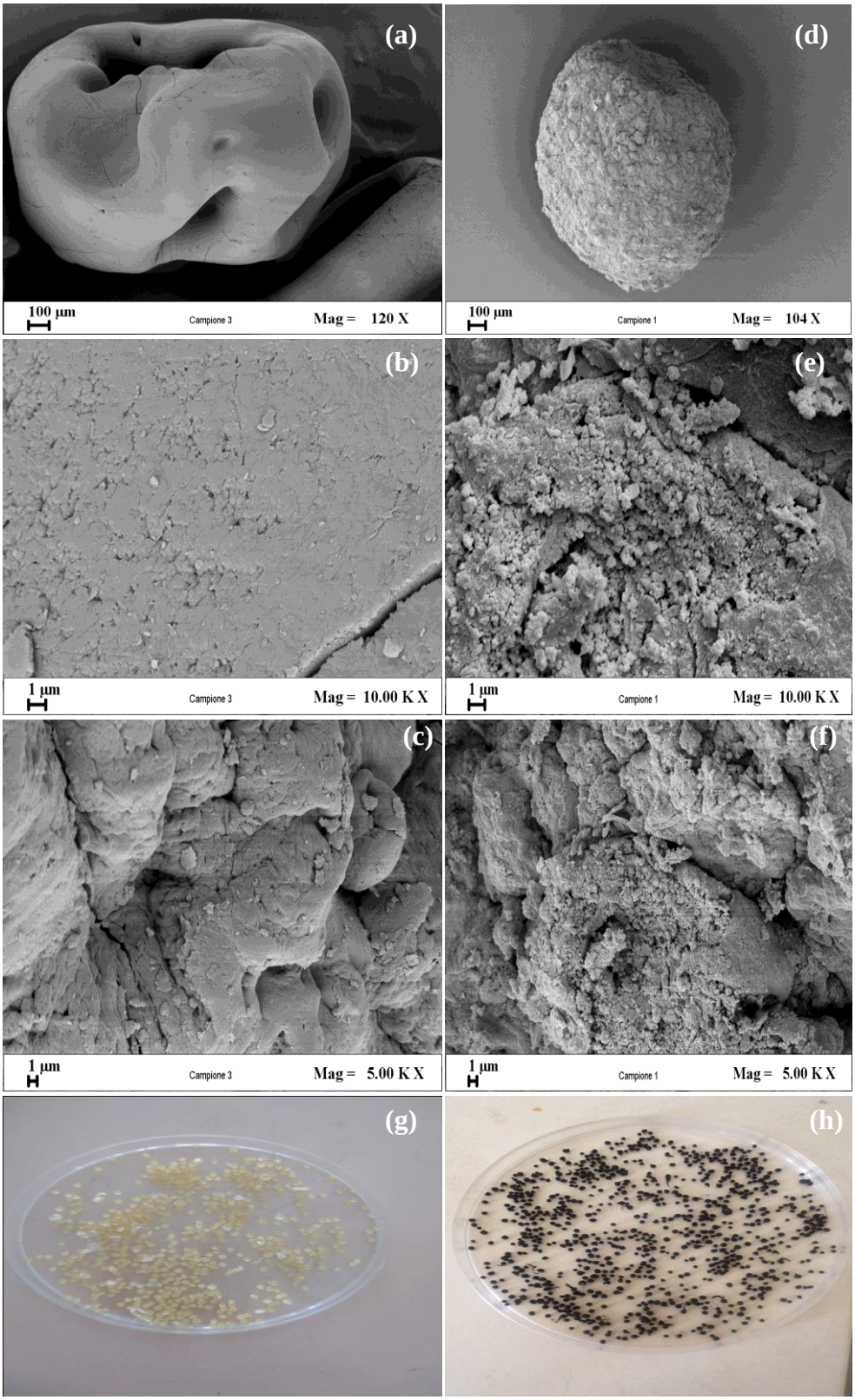

Figure 5: SEM images of pure calcium alginate beads at different magnifications (a-b-c), Fe_3O_4-NIO/calcium alginate beads at different magnifications (d-e-f) and digital photography of dry calcium alginate beads (g) and dry Fe_3O_4-NIO/calcium alginate beads (h).

Fe_3O_4-NIO/calcium alginate beads were characterized also by TEM. The results show irregular nanorods assigned to the natural iron ore [33], while the synthesized magnetic Fe_3O_4 nanoparticles display as spherical shape with an average diameter of 15 nm (Figure 6a, b), according to our previous study [33]. These well-distributed morphologies in the biopolymer matrix also confirm the incorporation of both used materials into the calcium alginate beads. EDX analysis of the hybrid nanocomposite beads surface confirms the presence of Na, Ca, Fe, O and Si elements in the prepared beads where Na, Ca are issued from sodium alginate and $CaCl_2$, respectively and Fe, O and Si are issued from natural iron oxide and the prepared magnetic nanoparticles (Figure 6c). Other elements were detected as traces like Cl, which could be due to non-completed removal of the $CaCl_2$ excess during the beads washing step. Moreover, detected copper and carbon are assigned to the carbon-coated copper grid utilized during the analysis. These findings further support the good embedding of both materials into the calcium alginate beads and the successful synthesis of Fe_3O_4-NIO/calcium alginate beads.

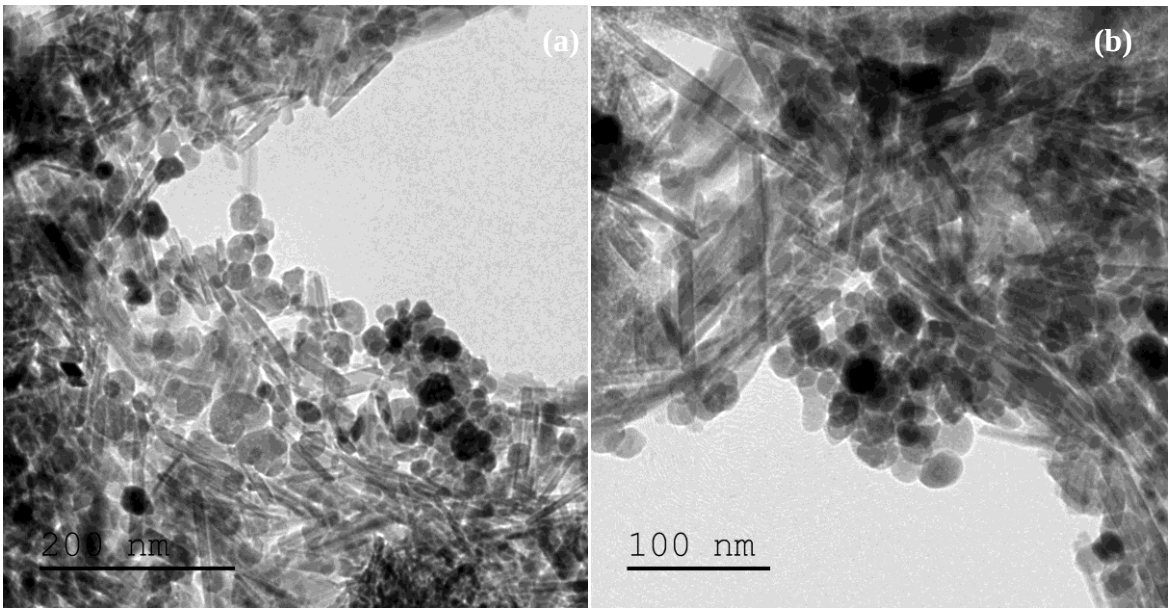

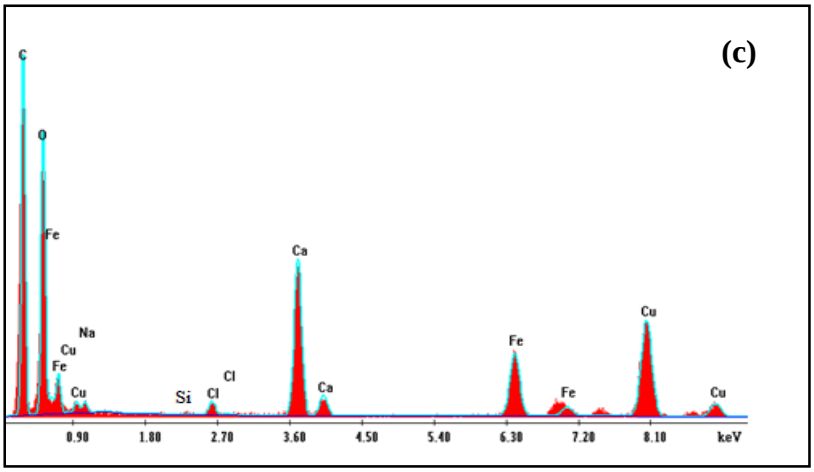

Figure 6: TEM micrographs of Fe_3O_4-NIO/calcium alginate beads at different scales: 200 nm (a), 100 nm (b), and its EDX spectrum (c).

3.1.4 Specific surface area and porosity

Porosity properties of bare calcium alginate beads and the hybrid nanocomposite beads were investigated using the N_2 adsorption–desorption experiments and the obtained results are summarized in the Table 1. Based on the BET method, the specific surface area of bare calcium alginate beads and Fe_3O_4-NIO/calcium alginate beads were found to be about 2 m^2/g and 26 m^2/g, respectively. Total volume pore (V_t) and the average pore diameter of both materials were determined by BJH method (Table 1). The prepared Fe_3O_4-NIO/calcium alginate beads resulted in a surface area higher than the bare beads and this increase is due to the embedding of Fe_3O_4 nanoparticles and the natural iron oxide into the beads that increased the pores. These findings are in good agreement with the SEM observations. It is also worthy to mention that a higher surface area could provide more adsorptive and catalytically active binding sites leading to an efficient degradation of the target contaminant [56]. Moreover, results reveal that both investigated materials are mesoporous according to pore size classification of IUPAC, since they show an average pore diameter of about 19 nm.

Table 1: textural characteristics of the pure calcium alginate beads and Fe_3O_4-NIO/calcium alginate beads.

Material	Specific surface area (m^2/g)	Total volume pore (cm^3/g)	Average pore diameter (nm)
Bare calcium alginate beads	2	0.001046	18.87
Fe_3O_4-NIO/calcium alginate beads	26	0.037347	18.82

3.1.5 Diffuse reflectance spectroscopy

The optical absorption properties of the prepared beads were evaluated through UV–vis DRS in the range 200–600 nm. These results show strong adsorption in the visible region. However, it is possible to observe that the light absorption edge is located in the UV region at about 255 nm (Figure7), in agreement with a previous study [57] and making the photocatalyst an effective candidate for water treatment under a wide region, including UV and solar light irradiations. Moreover, the optical band energy (Figure7 inset) was found to be 1.7 eV. Since the investigated photocatalyst showed an absorption edge located in the UV region, a UV-C lamp was used as light source in the photocatalytic tests.

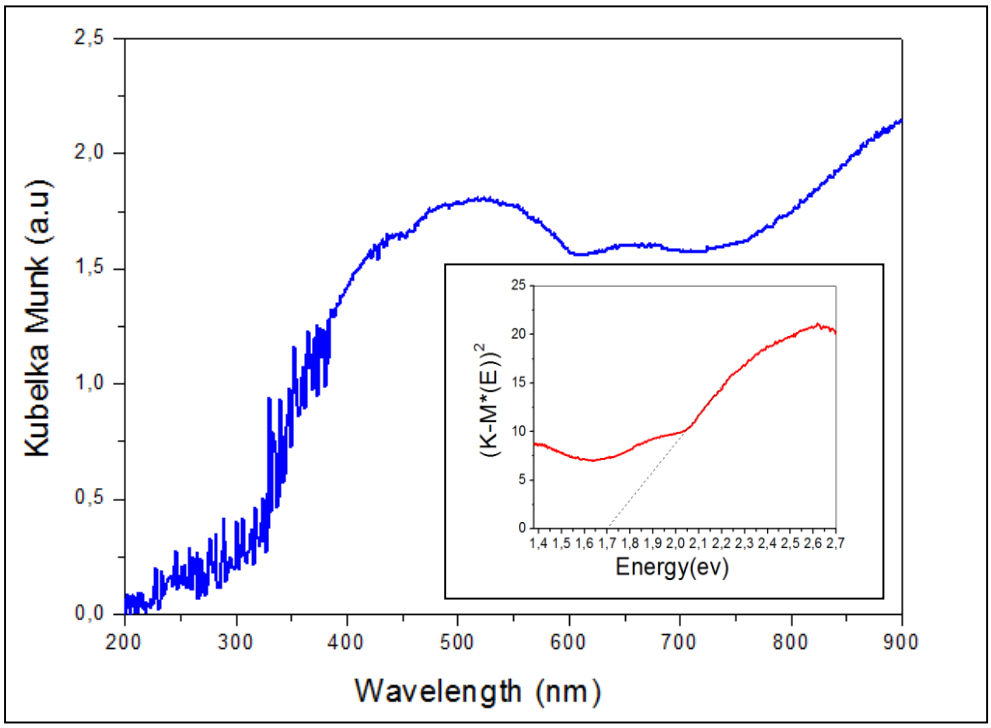

Figure 7: UV-Vis DRS spectra and bandgap evaluation (inset figure) of Fe_3O_4-NIO/calcium alginate beads.

3.2. Novacron blue dye degradation

3.2.1. Effect of differents parameters on NB dye removal by adsorption onto Fe_3O_4-NIO/calcium alginate beads

In order to determine the required time to reach the equilibrium condition, 100 mL of NB dye (40 mg/L), at spontaneous pH (6.9), was mixed with 0.1g of the hybrid magnetic beads in the dark for 120 min and the dye removal was very poor (~3%).

The pH of the medium is expected to strongly affect the adsorption of dye onto the beads surface through (i) the protonation or deprotonation of the beads surface, (ii) the dye chemistry and thereby (iii) the interaction between the dye molecules and the functional groups (hydroxyl and carboxyl groups) on the surface of the biopolymer. Hence, the effect of pH was investigated by keeping the above mentioned parameters constants while varying the pH in the range 2-8. When the pH of the dye solution decreased from 8 to 2, the percentage of dye removal increased up to 17.5% within 60 min (Figure 8a). This can be explained by the fact that, at very acidic conditions, the surface of the beads is positively charged and the interaction between the protonated carboxyl groups and dye molecules is favorable. Thereby, the adsorption of NB dye onto the beads is favored at pH 2 and this optimum pH was used in the subsequent experiments. This outcome is consistent with the result reported by De Assis et al [2] about the degradation of NB dye by TiO_2/palygorskite nanocomposite. Furthermore, many studies proved that alginate may be degraded by OH radicals during AOPs under pH> 5[38, 58] and this supports/strengthens the use of pH 2 since that Fe_3O_4-NIO/ calcium alginate beads was used as a catalyst in Fenton and photo-Fenton processes.

The increase of the magnetic beads mass from 0.1g to 0.2g led to the enhancement of the removal efficiency from about 18% to 22% (Figure8b), as a result of the increased available surface area and the existence of more free active sites [59,60]. Nevertheless, increasing the as-synthesized beads dose above 0.2g causes a reduction in removal efficiency. This may be due to the saturation of available sites as a result of the decrease in the dye molecules/adsorbent ratio [61].

The effect of NB dye initial concentration on the adsorption efficiency was also investigated (Figure8c). An increase in NB removal percentage from 13% to 18% occurs when the dye concentration was increased from 10 mg/L to 40 mg/L. Thus, the initial concentration of NB dye was found to be a driving force in the adsorption process [62]. Consequently, the optimum conditions (pH 2, $[NB]_0$= 40mg/L and 0.2g dose of beads) were chosen for subsequent (photo) Fenton tests.

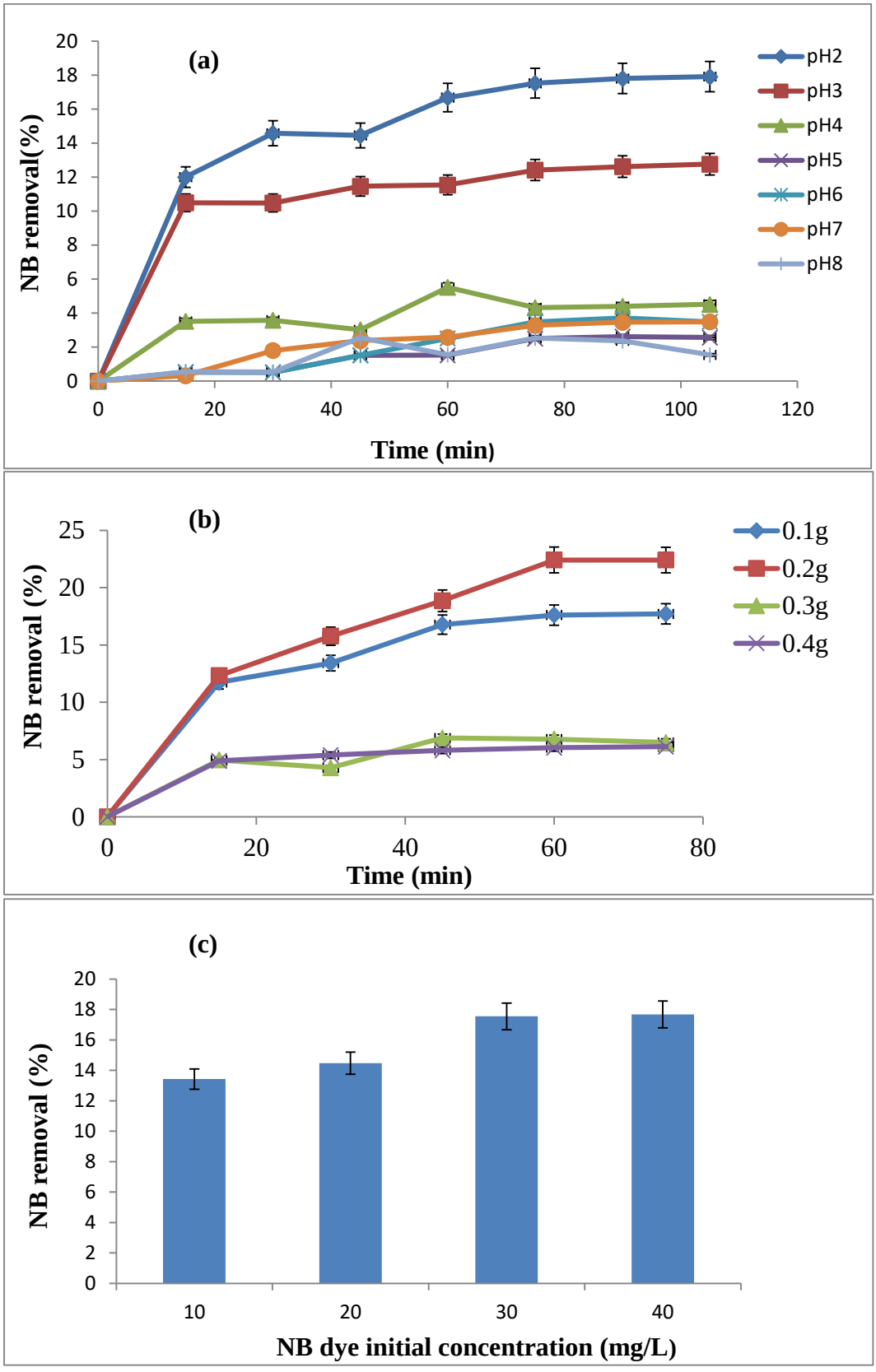

Figure 8: Effect of different parameters on NB dye adsorption: (a) pH, (b) mass of beads and (c) initial concentration of NB dye.

3.2.3. NB dye degradation via Fenton and photo-Fenton processes

The degradation of the NB dye under four different systems was investigated to discriminate the effect of Fenton and photo Fenton processes from the contributions of H_2O_2 and UV-C radiation, respectively (Figure9).

The direct oxidation by H_2O_2 was not able to degrade the NB dye. Similar result was reported by Martínez-López et al [63]. However, the photolysis process (UV-C irradiation alone) shows an enhancement of the NB dye degradation that reaches about 35% in 90 min. This result is also in agreement with a previous study [2] under the same conditions ([NB]=40 mg/L, pH 2 and UV-C irradiation).

For Fenton process (H_2O_2/catalyst in the dark), H_2O_2 was added to the solution after 60 min of dark adsorption. The process was conducted under different hydrogen peroxide concentrations (1, 2 and 5mM) to determine the adequate dose of H_2O_2.The increase in H_2O_2 concentration from 1 to 5mM (Figure10.a) led to an improved removal efficiency from 35% to 50% after 120 min of Fenton process, consistently with the scientific literature [64, 65, 66, 67]. This is possible due to the higher generation of ·OH coming from the decomposition of H_2O_2 catalyzed by Fe^{2+} loaded in the beads (Equation (1)). These generated radicals were able to attack NB dye molecules (Equation(8)). It is worth noting that the increase of H_2O_2 concentration up to 5 Mm led to a faster NB dye degradation in the early 40 min, reaching about 43% removal compared to only 26% observed for 1 or 2mM of H_2O_2 dose. Moreover, 1mM and 2 mM of H_2O_2 were totally consumed to reach only 35% of NB dye removal, indicating the production of an insignificant amount of ·OH. However, at a higher concentration of hydrogen peroxide (5mM) (Figure10.b), the decomposition of H_2O_2 (H_2O_2 consumption) by the iron entrapped in the beads was faster and effective to produce a sufficient amount of ·OH in the first hour of the process. Hence, 5 mM of H_2O_2 was considered as the optimal dose and used in the photo Fenton tests. According to the scientific literature, many iron based catalysts succeeded to catalyze hydrogen peroxide for producing radicals to degrade organic pollutants [38, 68, 69, 70].

Photo Fenton ([NB] = 40mg/L, pH 2, dose of beads = 0.2g/L, [H_2O_2] =5mM and 120 min of UVC- irradiation) was found to be the most efficient process with 80% of dye removal after 120min of irradiation. A so high efficiency can be explained by production of holes and electrons due to the excitation of magnetic alginate beads under UV-C radiation (Equation (2)) [71]. Thereafter, these electrons will be captured by hydrogen peroxide, creating another path to generate OH radicals (Equation (3)) [64]. In addition to that, even the photogenerated holes

can contribute to the direct oxidation of the NB dye (Equation (4)) [64] or by reducing H_2O and hydrogen peroxide to produce more $^{\bullet}OH$ (Equation (5) and (6) [72,73]. Furthermore, the photolysis of hydrogen peroxide (Equation (7)) during photo-Fenton process can contribute to the production of radicals by dissociating O-O bond [74, 75].

$$Fe^{2+} + H_2O_2 \rightarrow Fe^{3+} + OH^- + {}^{\bullet}OH \quad (1)$$

Magnetic beads + $h\nu \rightarrow$ Magnetic beads ($h^+ + e^-$) (2)

$$e^- + H_2O_2 \rightarrow HO^- + HO^{\bullet} \quad (3)$$

$$h^+ + \text{NB dye} \rightarrow \text{NB degradation} \quad (4)$$

$$h^+ + H_2O \rightarrow H^+ + HO^{\bullet} \quad (5)$$

$$h^+ + HO^- \rightarrow HO^{\bullet} \quad (6)$$

$$H_2O_2 + h\nu \rightarrow 2\,{}^{\bullet}OH \quad (7)$$

$$^{\bullet}OH + \text{NB dye} \rightarrow + H_2O + \text{NB degradation} \quad (8)$$

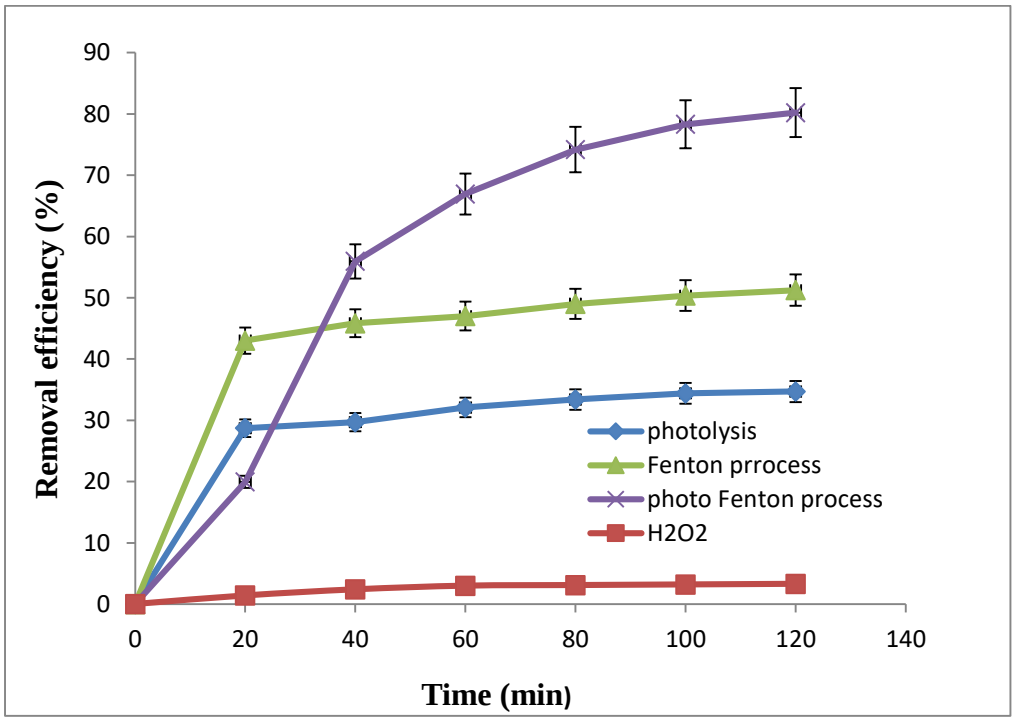

Figure 9: Degradtion of NB dye under different treatment conditions.

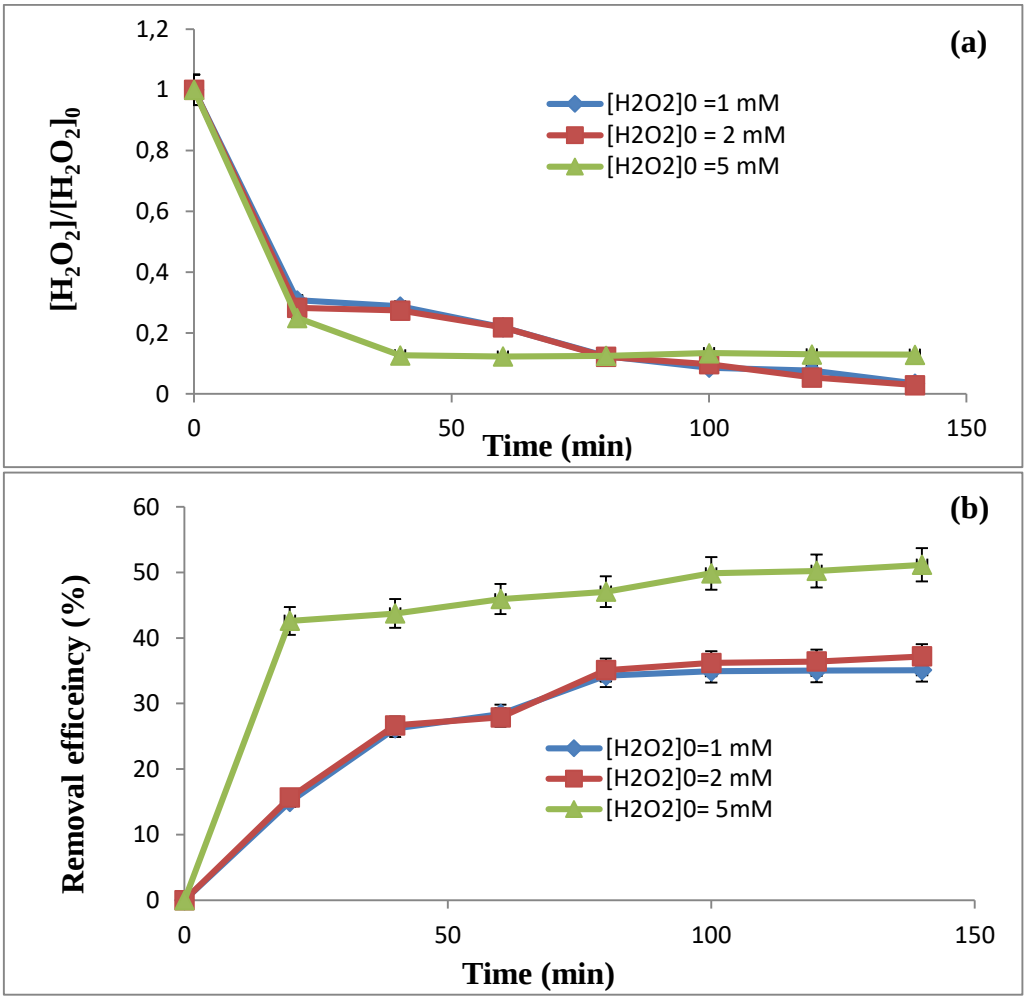

Figure 10: Effect of H_2O_2 initial concentration on **(a)** NB dye degradation and **(b)** the decomposition of hyrogen peroxide during Fenton process.

3.3. Reusability of the hybrid nanocomposite beads

Since the reusability of the catalyst is crucial with regard to possible application at industrial scale, six consecutive cycles of NB dye aqueous solution treatment by the photo-Fenton process were carried out. The nanocomposite beads were collected easily by a magnet and reused in the subsequent run. The removal efficiency of NB dye (80%) did not change in the first four consecutive runs (Figure11), suggesting an excellent reusability of the catalyst. However, a slight decrease in the removal efficiency was observed after the fourth cycle. This little decrease in the catalytic performance of the catalyst compared to its performance in the fourth run may be due to the iron leaching phenomenon or to a small depolyremization of the biopolymer matrix after been exposed to the UV-C light for a long time. Further investigations can be performed in the upcoming work. Nevertheless, the investigated catalyst maintains a good

catalytic performance to degrade NB dye in four subsequent cycles which makes it a potentially attractive option for real dyestuff wastewater treatment.

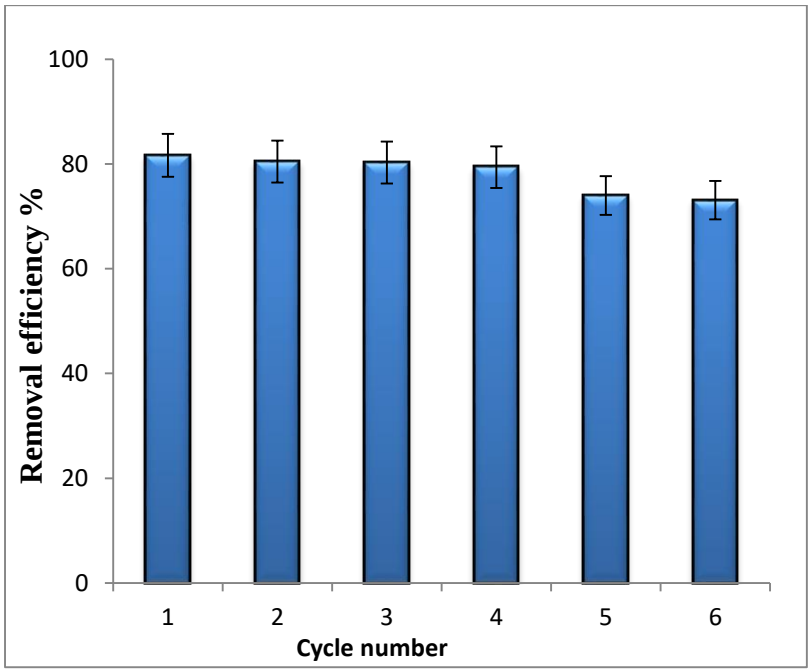

Figure 11: Efficiency of Fe_3O_4-NIO/calcium alginate beads on subsquent NB dye removal via photo Fenton process ([NB]= 40mg/L, pH2, mass of beads 0.2g, [H_2O_2]= 5mM and 120 min UV-C irradiation)

3.4. Comparison with the results of other biopolymer based catalysts available in the literature

Numerous biopolymer-based catalysts have been evaluated as AOPs in the degradation of dyes in previous studies and some of them are summarized in the Table 2 for comparison purpose with the catalyst investigated in the present work. Although no previous work on NB dye is available in the scientific literature, our catalyst can be competitive with similar catalysts investigated so far in terms of process efficiency, treatment time and stability. In addition, its simple and inexpensive preparation method, using less chemicals compared to the other catalysts, makes it more attractive for possible industrial scale-up.

Table 2: comparison of Fe_3O_4-NIO/calcium alginate beads with other biopolymer based catalysts existing in the literature.

Catalyst	Dye	Process and conditions	Degrad -ation (%)	Stability of the system	Refere-nce

Fe_3O_4@cellulose aerogel nanocomposite	Rhodamine B	Fenton-like reaction pH 3 $[H_2O_2]$= 9.9 mM, Catalyst dose 3 g/L, t= 64h	100%	Six cycles (97%-100% dye removal)	[76]
alginate/PVA hydrogel-supported magnetic Fe_3O_4 particles	methyloran ge	Heterogeneous Fenton pH 3 3mL of H_2O_2(30 wt %) Catalyst dose 1 g/L, t=25min	92 %	Six cycles (degradation reduced by 5.7% and 10% of catalyst mass loss)	[77]
Fe (III)-Cross-linked Alginate-Carboxymethyl cellulose composites	Malachite green	Photocatatlytic degradation UV-A light pH 4 Catalyst dose 1 g/L, t=30min	98%	~	[78]
Ag/AgCl@CMC hydrogel beads	Rhodamine B	Photocatalytic degradation pH 7 Catalyst dose 4 g/L, t= 60min	98 %	Five cycles (degradation decreased to 68 %)	[79]
ZnO/Fe_3O_4-Alginate beads	Reactive Red 180	Photocatalytic degradation UV-A light pH3 Catalyst dose 20g/L t= 60min	100 %	Ten cycles (maintain 100% of dye removal)	[52]
Fe_3O_4-NIO/Calcium alginate beads	Novacron blue	Photo Fenton pH 2 $[H_2O_2]$=5mM, Catalyst dose 2g/L UV-C light t=120min	80%	six cycles (degradation decreased to 73.1%)	Present work

4. Conclusion

Fe_3O_4- NIO/calcium alginate beads were successfully synthesized by a simple and effective method. These novel nanocomposite beads were characterized and tested as an adsorbent-catalyst for Novacron blue dye degradation. Taking advantage of the known adsorptive properties of the alginate (support), the incorporation of natural iron ore and

Fe_3O_4nanoparticlesinto the alginate support led to the synthesis of a good catalyst for Fenton and photo-Fenton processes. Moreover, its magnetic behavior derived from Fe_3O_4nanoparticlesmakes their removal (and recovery) easy after treatment. This novel heterogeneous catalyst succeeded to degrade 80% of NB dye within 120 min via photo-Fenton process under these optimum conditions: [NB]=40mg/L, pH 2, catalyst dose 2g/L $[H_2O_2]$=5mM, UVC light. Fe_3O_4-NIO/calcium alginate bead proves its ability to be reused for fourth consecutive cycles without any catalytic behavior loss. In summary, an ecofriendly, low cost and recyclable catalyst has been investigated and effectively used to remove a reactive azo dye from aqueous solution via photo-Fenton process, but the acidification cost should be taken into account in possible full scale applications when comparing this process with consolidated ones.

Acknowledgments

The authors would like to thank: (i) the Ministry of Higher Education and Scientific Research (Tunisia) for supporting the Sirine Ben Ayed's scientific stay in Salerno through a scholarship "Bourse d'alternance", (ii) the University of Salerno for the support through the project "Treatment of aqueous matrices using photo driven advanced oxidation processes" (FARB2021, ORSA219878); (iii) the King Saud University (Riyadh, Saudi Arabia) for the Research Supporting Project (RSP- 2021/75).

References

[1] D. Dahiya, P. S. Nigam, Waste management by biological approach employing natural substrates and microbial agents for the remediation of dyes' wastewater, Appl. Sci.10(8) (2020) 2958. https://doi.org/10.3390/app10082958

[2] M.L.M. De Assis, E.D. Junior, J.M.F. de Almeida, I. do Nascimento Silva, R.V. Barbosa, L.M. Dos Santos, C.A. Martinez-Huitle, Photocatalyticdegradation of Novacron blue and Novacronyellowtextiledyes by the TiO_2/palygorskitenanocomposite, Environ. Sci. Pollut. Res. 28(45) (2021) 64440-64460. 10.1007/s11356-021-15519-5

[3] F.E.F. Rêgo, A.M. Sales Solano, I.C. Da Costa Soares, D.R. da Silva, C.A.M. Huitle, M. Panizza, Application of electro-Fenton process as alternative for degradation of Novacron Blue dye, J Environ Chem Eng. 2(2014)875–880. https://doi. org/10.1016/j.jece.2014.02.017.

[4] A. Sakalis, D. Ansorgova, M. Holapek, P. Jandera A. Voulgaropoulos, Analysis of sulphonatedazodyes and their degradation products in aqueous solutions treated with a new electrochemical method, Intern. J. Environ. Anal. Chem. 84 (11) (2004) 875-888. https://doi.org/10.1080/03067310310001626731

[5] U. Pagga, D. Brown, The degradation of dyestuffs: part II behaviour of dyestuffs in aerobic biodegradation tests, Chemosphere. 15.4 (1986): 479-491https://doi.org/10.1016/0045-6535(86)90542-4

[6] Y.M. Slokar, A.M. Le Marechal, Methods of decoloration of textile wastewaters, Dyes Pigm. 37(1997) 335-356. https://doi.org/10.1016/S0143-7208(97)00075-2

[7] V.K. Gupta, Suhas, Application of low-cost adsorbents for dye removal, J. Environ. Manage. 90(8) (2009) 2313-2342. https://doi.org/10.1016/j.jenvman.2008.11.017

[8] S.Martínez-López, C. Lucas-Abellán, A. Serrano-Martínez, M.T. Mercader-Ros, N. Cuartero, P. Navarro, S. Pérez, J.A. Gabaldón, V.M. Gómez-López, Pulsed light for a cleaner dyeing industry: Azo dye degradation by an advanced oxidation process driven by pulsed light, J. Clean. Prod. 217 (2019) 757- 766. https://doi.org/10.1016/j.jclepro.2019.01.230.

[9] W. Xia, B. Song, H. Yi, E. Almatrafi, Y. Yang, Y. Fu, X. Huo, F. Qin, L. Xiang, Y. Zeng, G. Zeng, C. Zhou, From aquatic biota to autogenous N-doping biochar—using a highly efficient nonradical dominant process for sulfamethoxazole degradation, J. Clean. Prod. 373 (2022) 133750. https://doi.org/10.1016/j.jclepro.2022.133750

[10] C. Zhou, Y. Liang, W. Xia, E. Almatrafi, B. Song, Z. Wang, Y. Zeng, Y. Yang, Y. Shang, C. Wang, G. Zeng, Single atom Mn anchored on N-doped porous carbon derived from spirulina for catalyzed peroxymonosulfate to degradation of emerging organic pollutants. J. Hazard. Mater. 441 (2023) 129871. https://doi.org/10.1016/j.jhazmat.2022.129871

[11] C. Zhou, E. Almatrafi, X. Tang, B. Shao, W. Xia, B. Song, W. Xiong, W. Wang, H. Guo, S. Chen, G. Zeng, Investigation on the structure-performance of phthalic acid carboxyl position and carbon nitride towards efficient photocatalytic degradation of organic pollutants. Sep. Purif. Technol. 286 (2022) 120464. https://doi.org/10.1016/j.seppur.2022.120464

[12] N. Klamerth, L. Rizzo, S. Malato, M.I. Maldonado, A.Agüera, A.R. Fernández-Alba, Degradation of fifteen emerging contaminants at μg L^{-1} initial concentrations by mild solar photo-Fenton in MWTP effluents, Water Res. 44 (2010) 545-554https://doi.org/10.1016/j.watres.2009.09.059.

[13] J. Garcia-Montano, F. Torrades, J.A. Garcia-Hortal, X. Domenech, J. Peral, Degradation of Procion Red H-E7B reactive dye by coupling a photo-Fenton system with a sequencing batch reactor, J. Hazard. Mater B. 134 (2006) 220-229. https://doi.org/10.1016/j.jhazmat.2005.11.013

[14] L. Rizzo, S. Meric, D. Kassinos, M. Guida, F. Russo, V. Belgiorno, Degradation of diclofenac by TiO_2photocatalysis: UV absorbance kinetics and process evaluation through a set of toxicity bioassays,Water research. 43(4) (2009) 979-988. https://doi.org/10.1016/j.watres.2008.11.040

[15] A.Fiorentino, P. Prete, L. Rizzo, R. Cucciniello, A. Proto, Fe^{3+}- IDS as a new green catalyst for water treatment by photo-Fenton process at neutral pH, J Environ Chem Eng. 9 (6) (2021), 106802. 106802. https://doi.org/10.1016/j.jece.2021.106802

[16] J.P. Ribeiro, M.I. Nunes, Recent trends and developments in Fenton processes for industrial wastewater treatment – a critical review, Environ. Res. 197 (2021), 110957 https://doi.org/10.1016/j.envres.2021.110957

[17] S.B. Hammouda, F. Fourcade, A. Assadi, I. Soutrel, A. Amrane, L. Monser, Effective heterogeneous electro-Fenton process for the degradation of a malodorous compound, indole, using iron loaded alginate beads as a reusable catalyst, Appl. Catal.B: Environ, 182, (2016) 47-58.https://doi.org/10.1016/j.apcatb.2015.09.007

[18] R. C. C. Costa, F. C. C. Moura, P. E. F. Oliveira, F. Magalhães, J. D. Ardisson, R. M. Lago, Controlled reduction of red mud waste to produce active systems for environmental applications: heterogeneous Fenton reaction and reduction of Cr (VI), Chemosphere. 78 (2010) 1116 – 1120.https://doi.org/10.1016/j.chemosphere.2009.12.032

[19] M. Askarieh, H. Farshidi, A. Rashidi, A. Pourreza, M. S. Alivand, Comparative evaluation of MIL-101(Cr)/calcium alginate composite beads as potential adsorbents for removing water vapor from air, Sep. Purif. Technol. 291(2022) 120830. https://doi.org/10.1016/j.seppur.2022.120830

[20] A. A. Edathil, E. Alhseinat, F. Banat, Removal of heat stable salts from industrial lean methyldiethanolamine using magnetic alginate/iron oxide hydrogel composite, Int. J. Greenh. Gaz. Control. 83 (2019) 117-127. https://doi.org/10.1016/j.ijggc.2019.02.005

[21] B. Li, Y. Dong, C. Zou, Y. Xu, Iron (III)–alginate fiber complex as a highly effective and stable heterogeneous fenton photocatalyst for mineralization of organic dye. Ind. Eng. Chem. Res, 53(11) (2014) 4199-4206. https://doi.org/10.1021/ie404241r

[22] A. Atthanaphanit, P. Supaphol, H. Tamura, S. Tokura, R. Rujiravanit, Wet-spun alginate/chitosan whiskers nanocomposite fibers: Preparation, characterization and release characteristic of the whiskers, Carbohydr. Polym. 79 (2010) 738−746 .https://doi.org/10.1016/j.carbpol.2009.09.031

[23] T.Y. Kim, H.J. Jin, S.S. Park, S.J. Kim, S.Y. Cho, Adsorption equilibrium of copper ion and phenol by powdered activated carbon, alginate bead and alginate-activated carbon bead, J. Ind. Eng. Chem. 14(6) (2008) 714–719. 10.1016/j.jiec.2008.07.004

[24] G.T. Grant, E.R. Morris, D.A. Rees, P.J.C. Smith, D. Thom, Biological interactions between polysaccharides and divalent cations: The egg-box model, FEBS Lett. 32 (1) (1973) 195–198. 10.1016/j.jiec.2008.07.004

[25] B. B. Mandal, S.C. Kundu, Calcium alginate beads embedded in silk fibroin as 3D dual drug releasing scaffolds, Biomaterials, 30(28) (2009) 5170-5177. https://doi.org/10.1016/j.biomaterials.2009.05.072

[26] S.I. Somo, O. Khanna, E.M. Brey, Alginate microbeads for cell and protein delivery. Cell Microencapsulation, Humana Press, New York, NY, 2017, pp.217- 224. 10.1007/978-1-4939-6364-5_17

[27] K.Won, S. Kim, K. J. Kim, H. W. Park, S. J. Moon, Optimization of lipase entrapment in Ca-alginate gel beads, Process biochem. 40(6) (2005) 2149-2154. https://doi.org/10.1016/j.procbio.2004.08.014

[28] M. Nithya, K. Praveen, U.N. Sathya Balasubramanian, A. Pandurangan, Green synthesis of α-Fe_2O_3/$BiPO_4$ composite and its biopolymeric beads for enhanced photocatalytic application, J. Mater. Sci.: Mater. Electron. 29(17) (2018) 14733-14745. https://doi.org/10.1007/s10854-018-9610-2

[29] A. Idris, N.S.M. Ismail, N. Hassan, E. Misran, A.F. Ngomsik, Synthesis of magnetic alginate beads based on maghemite nanoparticles for Pb (II) removal in aqueous solution, J. Ind. Eng. Chem. 18(5) (2012)1582-1589. https://doi.org/10.1016/j.jiec.2012.02.018

[30] D. Peramune, D.C. Manatunga, R.S. Dassanayake, V. Premalal, R.N. Liyanage, C. Gunathilake, N. Abidi, Recent advances in biopolymer-based advanced oxidation processes for dye removal applications: A review,Environ. research, 215 (2022). 114242. https://doi.org/10.1016/j.envres.2022.114242

[31] S. Gautam, P. Shandilya, B. Priya, V.P. Singh, P. Raizada, R. Rai, M.A. Valente, P. Singh, Superparamagnetic $MnFe_2O_4$ dispersed over graphitic carbons and composite and bentonite as magnetically recoverable photocatalyst for antibiotic mineralization, Separ. Purif. Technol. 172 (2017) 49-511. https://doi.org/10.1016/j.seppur.2016.09.006

[32] L. Josephson, J.M. Perez, R. Weissleder , Magnetic nanosensors for the detection of oligonucleotide sequences., AngewChemInt Ed. 40 (2001) 3204.

[33] S. Ben Ayed, H.M. Sbihi, M. Azamb, S.I. Al-Resayes, M.T. Ayadi, F. Ayari, Local iron ore identification: comparison to synthesized Fe_3O_4 nanoparticles obtained by ultrasonic assisted reverse co-precipitation method for Auramine O dye adsorption, DESALIN WATER TREAT. 220 (2021) 446–458. doi: 10.5004/dwt.2021.27080

[34] J.P. Paques, E. Van der Linden, C.J.M. van Rijn, L.M.C. Sagis, Alginate submicron beads prepared through w/o emulsification and gelation with $CaCl_2$nanoparticles,FoodHydrocoll. 31 (2013) 428–434.https://doi.org/10.1016/j.foodhyd.2012.11.012

[35] S.Barreca, J.I.V. Colmenares, A. Pace, S. Orecchio, C. Pulgarin, Neutral solar photo-Fenton degradation of 4-nitrophenol on iron-enriched hybrid montmorillonite-alginate beads (Fe-MABs), J. Photochem. Photobiol. A: Chem. 282 (2014) 33-40 https://doi.org/10.1016/j.jphotochem.2014.02.008

[36] M. Kumar, G. Vijayakumar, R. Tamilarasan, Synthesis, characterization and experimental studis of nano Zn–Al–Fe_3O_4 blended alginate/Ca beads for the adsorption of rhodamin B, *J. Polym. Environ.* 27(1) (2019) 106-117. https://doi.org/10.1016/j.jphotochem.2014.02.008

[37] H. Zeng, S. Sun, K. Xu, W. Zhao, R. Hao, J. Zhang, D. Li, Iron-loaded magnetic alginate-chitosan double-gel interpenetrated porous beads for phosphate removal from water: Preparation, adsorption behavior and pH stability, Reactive and Functional Polymers. React. Funct. Polym**.** 27 (2022) 106-117. https://doi.org/10.1007/s10924-018-1318-0

[38] R.F. Quadrado, A.R. Fajardo, Fast decolorization of azo methyl orange via heterogeneous Fenton and Fenton-like reactions using alginate-Fe^{2+}/Fe^{3+} films as catalysts, Carbohydr. Polym. 177 (2017) 443-450. 10.1016/j.carbpol.2017.08.083

[39] R. da Silva Fernandes, M.R. de Moura, G.M. Glenn, F.A. Aouada, Thermal, microstructural, and spectroscopic analysis of Ca^{2+} alginate/clay nanocomposite hydrogel beads, J. Mol. Liq. 265 (2018) 327-336.https://doi.org/10.1016/j.molliq.2018.06.005

[40] X. Gao, J. Liu, M. Li, C. Guo, H. Long, Y. Zhang, L. Xin, Mechanistic study of selective adsorption and reduction of au (III) to gold nanoparticles by ion imprinted porous alginate microspheres, Chem. Eng. J. 385 (2020), 123897. https://doi.org/10.1016/j.cej.2019.123897

[41] R.P. Medina, E.T. Nadres, F.C. Ballesteros, D.F. Rodrigues, Incorporation of graphene oxide into a chitosan–poly(acrylic acid) porous polymer nanocomposite for enhanced lead adsorption, Environ. Sci. Nano 3 (3) (2016) 638–646. https://doi.org/10.1016/j.ijbiomac.2022.07.238

[42] A. M. Awwad, N.M Salem, A green and facile approach for synthesis of magnetite nanoparticles, J. Nanosci. Nanotechnol. 2(6) (2012)208-213. 10.5923/j.nn.20120206.09

[43] H.B. Quesada, L.F. Cusioli, C.O. Bezerra, A.T.A. Baptista, L. Nishi, R.G. Gomes, R. Bergamasco, Acetaminophen adsorption using a low-cost adsorbent preparedfrom modified residues of Moringaoleifera Lam. seed husks, J. Chem. Technol. Biotechnol. 94 (2019) 3147–3157. https://doi.org/10.1002/jctb.6121

[44] J. Nastaj, A. Przewłocka, M. Rajkowska-My´sliwiec, Biosorption of Ni(II), Pb(II) and Zn(II) on calcium alginate beads: equilibrium, kinetic and mechanism studies, Polish J. Chem. Technol. 18 (3) (2016) 81–87, https://doi.org/10.1515/pjct-2016- 0052

[45] I. Aswin Kumar, N. Viswanathan, Development and reuse of amine-grafted chitosan hybrid beads in the retention of nitrate and phosphate, J. Chem. Eng. Data. 63 (2018) 147–158. https://doi.org/10.1021/acs.jced.7b00751

[46] S. Ben Ayed, M. Azam, S.I. Al-Resayes, F. Ayari, L. Rizzo, Cationic Dye Degradation and Real Textile Wastewater Treatment by Heterogeneous Photo-Fenton, Using a Novel Natural Catalyst, Catalysts. 11 (2021)1358. https://doi.org/ 10.3390/catal11111358

[47] F.B. Li, X.Z. Li, C.S. Liu, T.X. Liu, Effect of alumina on photocatalytic activity of iron oxides for bisphenol A degradation, J. Hazard. Mater. 149 (2007) 199 207. https://doi.org/10.1016/j.jhazmat.2007.03.069

[48] K.V. Sri, A. Kondaiah, J.V. Ratna, A. Annapurna, Preparation and characterization of quercetin and rutincyclodextrin inclusion complexes, Drug Dev. Ind. Pharm. 33 (2007) 245–253. https://doi.org/10.1080/03639040601150195

[49] Y. Dong, W. Dong, Y. Cao, Z. Han, Z. Ding, Preparation and catalytic activity of Fe alginate gel beads for oxidative degradation of azo dyes under visible light irradiation, Catal. Today, 175 (1) (2011)346-355.https://doi.org/10.1016/j.cattod.2011.03.035

[50] C.Wang, G. Li, B. Karmakar, H.S. AlSalem, A.A. Shati, A.F. El-kott, F. Elsaid, M. Bani-Fwaz,A. Alsayegh, S. Alkhayyat, G.E.S. Batiha, Pectin mediated green synthesis of Fe_3O_4/Pectin nanoparticles under ultrasound condition as an anti-human colorectal carcinoma bionanocomposite, Arab. J. Chem. 15(6) (2022) 103867. https://doi.org/10.1016/j.arabjc.2022.103867

[51] P. Karthikeyan, S. Meenakshi, Fabrication of hybrid chitosan encapsulated magnetic-kaolin beads for adsorption of phosphate and nitrate ions from aqueous solutions, Int. J. Biol. Macromol. 168 (2021) 750-759.https://doi.org/10.1016/j.ijbiomac.2020.11.132

[52] Z. Bilici, Z. Işık, Y. Aktaş, H.C. Yatmaz, N. Dizge, Photocatalytic effect of zinc oxide and magnetite entrapped calcium alginate beads for azo dye and hexavalent chromium removal from solutions, J. Water Process. Eng. 31(2019) 100826 https://doi.org/10.1016/j.jwpe.2019.100826

[53] Z. Isik, M. Saleh, N. Dizge, Adsorption studies of ammonia and phosphate ions onto calcium alginate beads,Surf. Interfaces. 26 (2021)101330 https://doi.org/10.1016/j.surfin.2021.101330

[54] R. Torres-Caban, C.A. Vega-Olivencia, N. Mina-Camilde, Adsorption of Ni^{2+} and Cd^{2+} from water by calcium alginate/spent coffee grounds composite beads, Appl. Sci. 9 (21) (2019), 4531. https://doi.org/10.3390/app9214531

[55] H. Kaygusuz, F.B. Erim, Alginate/BSA/montmorillonite composites with enhanced protein entrapment and controlled release efficiency, React. Funct. Polym. 73(11) (2013) 1420-1425. https://doi.org/10.1016/j.reactfunctpolym.2013.07.014

[56] V. Stengl, S. Bakardjieva, Molybdenum-doped anatase and its extraordinary photocatalytic activity in the degradation of orange II in the UV and Vis regions, J. Phys. Chem. C. 114 (2010)19308–19317. https://doi.org/10.1021/jp104271q

[57] M. Srivastava, J. Singh, M. Yashpal, M,Synthesis of superparamagnetic bare Fe_3O_4 nanostructures and core/shell (Fe_3O_4/alginate) nanocomposites, Carbohydr. Polym. 89(3) (2012) 821-829. https://doi.org/10.1016/j.carbpol.2012.04.016

[58] S.R. Mao, T.T. Zhang, W. Sun, X.H. Ren, The depolymerization of sodium alginate by oxidative degradation, Pharm. Dev. Technol. 17(6) (2012) 763–769. https://doi.org/10.3109/10837450.2011.583927

[59] A. A. Oladipo, M. Gazi, Enhanced removal of crystal violet by low cost alginate/acid activated bentonite composite beads: optimization and modelling using non-linear regression technique, J. Water Process. Eng, 2 (2014) 43-52. https://doi.org/10.1016/j.jwpe.2014.04.007

[60] Z. A. Zakaria, M. Suratman, N. Mohammed, W.A. Ahmed, Chromium (VI) removal from aqueous solution by untreated rubber wood sawdust. Desalination, 244 (2009)109–121.https://doi.org/10.1016/j.desal.2008.05.018

[61] D.L. Nunes, A.S. Franca, L.S. Oliveira, Use of Raphanussativus L. press cake, a solid residue from biodiesel processing, in the production of adsorbents by microwave activation. Environ. Technol. 32 (10) (2011) 1073 1083. https://doi.org/10.1080/09593330.2010.526965

[62] E. Alver, A.U. Metin, F. Brouers, Methylene blue adsorption on magnetic alginate/rice husk bio-composite, Int. J. Biol. Macromol. 154 (2020) 104 113. https://doi.org/10.1016/j.ijbiomac.2020.02.330

[63] S. Martínez-López, C. Lucas-Abellán, A. Serrano-Martínez, M.T. Mercader-Ros, N. Cuartero, P. Navarro, S. Pérez, J.A. Gabaldón, V.M. Gómez-López, Pulsed light for a cleaner dyeing industry: Azo dye degradation by an advanced oxidation process driven by pulsed light, J. Clean. Prod. 217 (2019) 757-766. https://doi.org/10.1016/j.jclepro.2019.01.230

[64] F. Mahmoudi, S. Farhadi, M. Jarosova, M. Sillanpää, Preparation of novel hybrid nanomaterials based on $LaFeO_3$ and phosphotungstic acid as a highly efficient magnetic photocatalyst for the degradation of methylene blue dye solution,Appl. Organomet. Chem, 34(12) (2020) 6011. https://doi.org/10.1002/aoc.6011

[65] I. Gulkaya, G.A. Surucu, F.B. Dilek, Importance of H_2O_2/Fe^{2+} ratio in Fenton's treatment of a carpet dyeing wastewater, J. Hazard. Mater. 136(3) (2006) 763-769. https://doi.org/10.1016/j.jhazmat.2006.01.006

[66] V. Kecić, D. Kerkez, M. Prica, O. Lužanin, M. Bečelić-Tomin, D.T. Pilipović, B. Dalmacija, Optimization of azo printing dye removal with oak leaves-nZVI/H_2O_2 system using statistically designed experiment. J. Clean. Prod.202 (2018) 65-80. https://doi.org/10.1016/j.jclepro.2018.08.117 /

[67] J. Zhong, B. Yang, Y. Feng, Y. Chen, L.G. Wang, W.D. You, G.G. Ying, Enhanced Photo–Fenton Removal Efficiency with Core-Shell Magnetic Resin Catalyst for Textile Dyeing Wastewater Treatment, Water, 13(2021) 968. https://doi.org/ 10.3390/w1307096

[68] N. Dai, S. Yi, X. Zhang, L. Feng, H. Ding, D. Song, X. Liu, J. Rao, Y. Zhang, Typical synthesis of an iron-modified Laponite @diatomite composite for photo-Fenton degradation of methyl orange dyes, Appl. Surf. Sci, 607(2022) 154886. https://doi.org/10.1016/j.apsusc.2022.154886

[69] N. Panda, H. Sahoo, S. Mohapatra, Decolourization of methyl orange using Fenton-like mesoporous Fe_2O_3-SiO_2 composite, J. Hazard. Mater.185(1) (2011) 359–365. https://doi.org/10.1016/j.jhazmat.2010.09.042

[70] S. Biswas, A. Pal, Iron oxide-loaded alginate-bentonite hydrogel beads as a green and sustainable catalyst for 4-nitrophenol reduction, Mater. Today. Commun. 28 (2021) 102588. https://doi.org/10.1016/j.mtcomm.2021.102588

[71] Q. Zhou, Y. Liu, G. Yu, F. He, K. Xiao, K. Chen, D. Xiao, J. Li, Degradation kinetics of sodium alginate via sono-Fenton, photo-Fenton and sono-photo-Fenton methods in the presence of TiO_2 nanoparticles, Polym. Degrad. Stab. 135 (2017) 111-120. https://doi.org/10.1016/j.polymdegradstab.2016.11.012

[72] T. Yang, J.L. Sun, L. Eriksson, G.B. Li, X.D. Zou, F.H. Liao, J.H. Lin, $Na_5[MB_{24}O_{34}(OH)_{12}]\cdot nH_2O$ ($M = Cr^{3+}Al^{3+}$): Unprecedented SpherelikePolyborate Clusters from Boric Acid Flux Synthesis, Inorg. Chem. 47 (2008) 3228–3233

[73] X. Zhang, Z.Geng, J. Jian, Y. He, .Z. Lv, X. Liu, H. Yuan, Potassium ferrite as heterogeneous photo-fenton catalyst for highly efficient dye degradation, Catalysts, 10(3) (2020) 293.

[74] Y. Wang, H. Song, J. Chen, S. Chai, L. Shi, C. Chen, C. He, A novel solar photo-Fenton system with self-synthesizing H_2O_2: enhanced photo-induced catalytic performances and mechanism insights, Appl. Surf. Sci.512 (2020). 145650 https://doi.org/10.1016/j.apsusc.2020.145650

[75] L.Clarizia, D. Russo, I. Di Somma, R. Marotta, R. Andreozzi, Homogeneous photoFenton processes at near neutral pH: a review, Appl. Catal. B: Environ. 209(2017)358–371. https://doi.org/10.1016/j.apcatb.2017.03.011

[76] Y. Jiao, C. Wan, W. Bao, H. Gao, D. Liang, J. Li, Facile hydrothermal synthesis of Fe_3O_4@cellulose aerogel nanocomposite and its application in Fenton-like degradation of Rhodamine B, Carbohydr. Polym. 189 (2018). 371-378. https://doi.org/10.1016/j.carbpol.2018.02.028

[77] M. Zhang, X. Ling, X. Zhang, G. Han, A novel alginate/PVA hydrogel -supported Fe_3O_4 particles for efficient heterogeneous Fenton degradation of organic dyes, Colloids

740 Surf. A Physicochem, Eng. Asp. 652 (2022) 129830.
741 https://doi.org/10.1016/j.colsurfa.2022.129830

742 [78] D. Karadeniz, N. Kahya, F.B. Erim, Effective photocatalytic degradation of malachite
743 green dye by Fe (III)-Cross-linked Alginate-Carboxymethyl cellulose composites, J.
744 Photochem. Photobiol. A: Chem, 428 (2022) 113867.
745 https://doi.org/10.1016/j.jphotochem.2022.113867

746 [79] H. Heidarpour, M. Golizadeh, M. Padervand, A. Karimi, M. Vossoughi, M.H. Tavakoli,
747 In-situ formation and entrapment of Ag/AgClphotocatalyst inside cross-linked carboxymethyl
748 cellulose beads: A novel photoactive hydrogel for visible-light-induced photocatalysis, J.
749 Photochem. Photobiol. A: Chem . 398 (2020) 112559.
750 https://doi.org/10.1016/j.jphotochem.2020.112559